Light interaction with AlN-based SAW device fabricated on flexible and silicon substrate

Leonardo Lamanna[*,1,2,3], Francesco Rizzi[1], Massimo De Vittorio[1,2], Venkat R. Bhethanabotla[*,3].

[1] *Center for Biomolecular Nanotechnologies, Istituto Italiano di Tecnologia, Via Barsanti snc, Arnesano, Italy*
[2] *University of Salento, Department of Innovation Engineering, Campus Ecotekne, Via Monteroni, Lecce, Italy*
[3] *Department of Chemical & Biomedical Engineering University of South Florida Tampa, USA*

[*] *leonardo.lamanna@iit.it; bhethana@usf.edu*

***Abstract*—The electroacoustic photoresponse of surface acoustic wave (SAW) delay line device, based on piezoelectric aluminum nitride (AlN) thin film sputtered on silicon rigid substrate and flexible polyethylene naphthalate (PEN) substrate, has been investigated. The electroacoustic response of SAW devices has been analyzed by measuring the transfer function S_{21} under light stimulus of different wavelengths. The S_{21} out-of-band insertion loss of SAW devices fabricated on silicon is strongly influenced by the photovoltaic effect when the devices are stimulated by light. A mathematical model has been implemented to correlate the out-of-band loss with the material's electrical admittance. The frequency shift of the resonance frequency modes (Rayleigh and Lamb) has also been characterized for both SAW devices on silicon and PEN substrates, when exposed to UV light. To the best of our knowledge, this is the first detection of UV light by a flexible AlN based SAW device. Further development of these devices exploiting electroacoustic photoresponse phenomena could lead to a new class of remote SAW devices as light sensors in the range between UV to IR.**

Keywords— AlN thin film, UV-IR sensing, flexible SAW devices.

I. INTRODUCTION

Surface acoustic wave (SAW) devices represent one of the most widely used micro electro mechanical systems (MEMS). The versatility of application of the SAW device, as well as low cost, small size, high reliability and good reproducibility of the RF output signal allows remote wireless control [1, 2]. SAW devices fabricated on piezoelectric thin films represent the most promising technology easily integrable in sensors, transducers, and lab on chip systems [3]. The main materials involved in this class of devices are zinc oxide (ZnO) and aluminum nitride (AlN). In particular, AlN represents an excellent substrate for the SAW device microfabrication thanks to good piezoelectric and dielectric properties, complementary-metal-oxide-semiconductor (CMOS) -based processing compatibility and biocompatibility [3,4]. Moreover, the high SAW propagation velocity and high breakdown voltage allow the fabrication of devices working with high power and in the GHz range [3,5]. Improvement in the sputtering technique now allow deposition of c-axis orientated AlN films at low temperature on different substrates such as sapphire [6], $LiNbO_3$ [7], silicon [8] and polymers [5]. The modes and amplitude of the waves propagation in the AlN-based SAW device, are strictly related to the electrical and mechanical properties of the substrate [3,5].

In this work, the interaction of light radiation with two different AlN-based SAW devices has been investigated: one fabricated on a silicon substrate and the other fabricated on a flexible polyethylene naphthalate (PEN) substrate. Silicon is the most common substrate used in integrated electronics; it is a semiconductor with bandgap around 1.14 eV [9,10]. Therefore, this material, if stimulated at the correspondent radiation frequency, shows a photovoltaic effect with a consequent resistivity change [11]. The resistivity change of the substrate influences the SAW device performance, mostly due to the electrical feedthrough between the interdigital transducers (IDTs), which considerably change the out-of-band signal [8]. In a sinusoidal voltage regime (AC circuits), where the SAW device is exploited, the resistance is described as a complex impedance or admittance [12]. In this study, the change of the admittance has been reported as a function of the different wavelength stimulus. Since the transmission signal S_{21} is influenced by feedthrough in the silicon substrate, a theoretical model has been developed to parameterize the out-of-band insertion loss with the characteristic material admittance. This behavior has been compared with SAW devices fabricated on polymeric PEN substrate, whose electrical properties are not affected by light stimulation. Finally, AlN light sensitivity has been investigated, as well. Piezoelectric AlN in a wurtzite phase shows a bandgap around 6 eV and it absorbs radiation in the UV light range [13]. Devices stimulated by UV light have shown a change in the resonance frequency due to the screening of the piezoelectric fields with a consequent reduction of the acoustic velocity [14].

The knowledge and development of theoretical models for SAW devices sensitive to different radiation intensities and wavelengths could enable a new class of remote devices that will find application in different fields such as flame monitors, sunlight exposure meters, photochemical phenomena detectors, etc.

II. MATERIALS

Silicon (1000 Ω/cm) with a top layer of SiN (10000 Ω/cm) substrate was purchased from Si-Mat; PEN film of 125 µm thickness was purchased from Teonex. The light sources used in the work are LEDs of wavelengths: 365nm (code M365LP1), 530nm (code M530L4), 660nm (code M660L4) and 940 nm (code M940L3) all purchased from Thorlabs. The LEDs were controlled by a T-Cube™ LED Driver purchased from Thorlabs. The power of the light source for the different wavelength is reported according to Thorlabs datasheet in Table 1.

978-1-7281-1634-1/19/$31.00 ©2019 IEEE

TABLE I. LEDS WAVELENGTHS, EQUIVALENT EV ENERGY AND LEDS OUTPUT POWER IN ACCORDING TO THORLABS DATASHEETS.

nm	eV	mW
365	3.5	1150
530	2.4	350
660	1.9	940
940	1.3	800

III. FABRICATION AND EXPERIMETN

The AlN deposition was carried out according to Lamanna et al. [5]. The devices used in the present study are delay lines constituted by two identical metal interdigital transducers (IDT) whose purpose is the generation of the SAWs. In detail, on silicon we have the generation of the Rayleigh wave whereas in the flexible PEN substrate we have two SAW modes of propagation (Rayleigh and Lamb) [3,5]. Each delay line is designed with 40 pairs of fingers, λ=20μm with a metallization ratio of 0.5, an acoustic aperture of 400 μm and a delay line of 20 λ. The microfabrication of the IDTs pattern is improved with respect to the previous work, exploiting a lift-off photolithography process using AZ 5214 E Image Reversal Photoresist. The metallization was carried out with a thermal evaporator using aluminum pellets (99.95% pure) with a final thickness of around 1000 Angstroms.

The experimental set up, used to study the electroacoustic photoresponse of the SAW devices, is shown in Fig.1a; additionally, Figs.1b,c show a 3-dimensional representation of the rigid and flexible characterized SAW devices. The light source was fixed at 3 cm from the delay line. The transfer function S_{21} has been obtained at room temperature with a vector network analyzer (Agilent 8753ES) using |Z|Probe with 150 μm pitch.

IV. MODELING

To characterize the out-of-band signal as a function of the incident light and therefore exploiting the electrical admittance, the model proposed by Clement et al. [8] was implemented for the present purpose. The admittance coefficient for a delay line spaced by nλ is given by:

$$Y_{11=}Y_{22} = G + j(B + \omega_0 C_{tot}) \quad (1)$$

$$Y_{21=}Y_{12} = G + exp(-j\,\omega_0 \frac{n\lambda}{f_0}) \quad (2)$$

$$G = {}^{4}/_{\pi}\, k^2\, \omega_0\; C_{tot}\, N\, (\frac{\sin(x)}{x})^2 \quad (3)$$

$$B = {}^{4}/_{\pi}\, k^2\, \omega_0\; C_{tot}\, N\, (\frac{\sin(2x)-2x}{2x^2}) \quad (4)$$

where B is the conductance, G is susceptance, C_{tot} is the IDT capacitance empirically fitted, ω the angular frequency, ω_0 angular resonance frequency, N pair of finger, K^2 is the electromechanical coupling equal to 0.85 as calculated in the previous work [5] and x is calculated as $[N\pi((\omega-\omega_0)/\omega_0)]$.

The transfer function S_{21} is given by:

$$S_{21} = \frac{-2\,Y_{21}Y_0}{(Y_0+Y_{11})^2-Y_{21}^2} \quad (5)$$

where Y_0 represents the admittance in agreement with the experimental setup. To fit the experimental data with the mathematical model, the feedthrough has to be calculated. According to [8] these effects can be approximated by adding a real term Y_P to Y_{12} parameter, which is equivalent to a purely resistive admittance in parallel. In an ideal case with a zero resistive admittance of the material, the response is a perfect sinc function signal (Fig.3a).

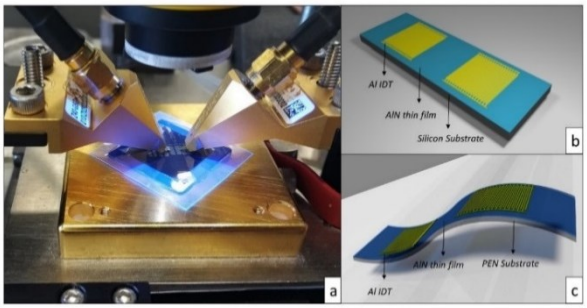

Fig. 1: Experimental set up for electroacoustic photoresponse test; b,c) 3D schematic of the developed AlN-based SAW device on Silicon and flexible Polyethylene Naphthalate substrate, respectively.

V. DISCUSSION

The characterization of the transfer functions S_{21} is reported in Fig. 2. The SAW devices fabricated on silicon substrate show a Raleigh mode of propagation (Fig.2a) with a resonant frequency of 250 MHz. Instead, the SAW devices fabricated on PEN (Fig.2b) exhibit two resonance modes: Rayleigh at a lower frequency (187 MHz) and symmetric Lamb S_0 at a higher frequency (505 MHz), in accordance with the previous work and the theoretical wave velocity [5]. Fig. 2a shows how the exposure of the silicon-SAW devices at different wavelengths changes the out-of-band insertion loss. The out-of-band insertion loss is dependent on the wavelength of light, and in particular, the increase in wavelength leads to an increase in the out-of-band losses. In fact, the silicon bandgap is 1.14eV (1080 nm) and the promotion of the electron in the conductance band is favored when the incident wavelength is closer to the bandgap energy (in the present work, the radiation is at 940nm) [15,16]. Therefore, the increasing of the out-of-band losses is caused by the promotion of the electrons to the conduction band at higher wavelengths and by the consequent increasing of the electrical feedthrough between the IDTs. This effect is not present in the devices fabricated on PEN polymeric substrate, transparent to this radiation wavelengths range and therefore not showing out-of-band insertion loss changes (Fig. 2b). Fig.3 shows the S_{21} spectra measured with different incident light stimuli and the relative S_{21} simulated spectra with different resistive admittance added to an ideal AlN-based SAW filter on silicon. The theoretical model perfectly fits the experimental data. This simple model provides valuable information about the change of electrical property of the substrate. In fact, it shows how the substrate admittance changes in a range between 0.8 10^{-5} Ω^{-1} to 2 10^{-4} Ω^{-1} when it is stimulated by different wavelengths LED sources. This variation is in accordance with the literature [17, 18].

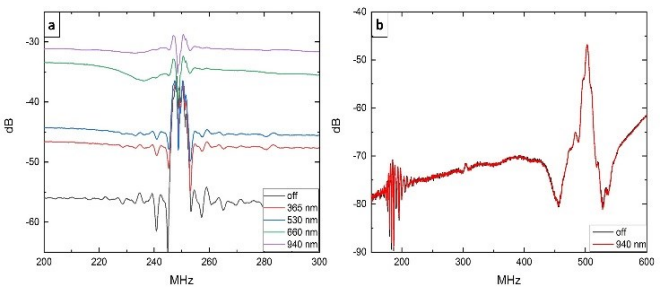

Fig. 2: Transfer function amplitude S_{21} a) devices fabricated on silicon substrate stimulated by different wavelengths light; b) devices fabricated on PEN substrate without light exposure and stimulated by IR light.

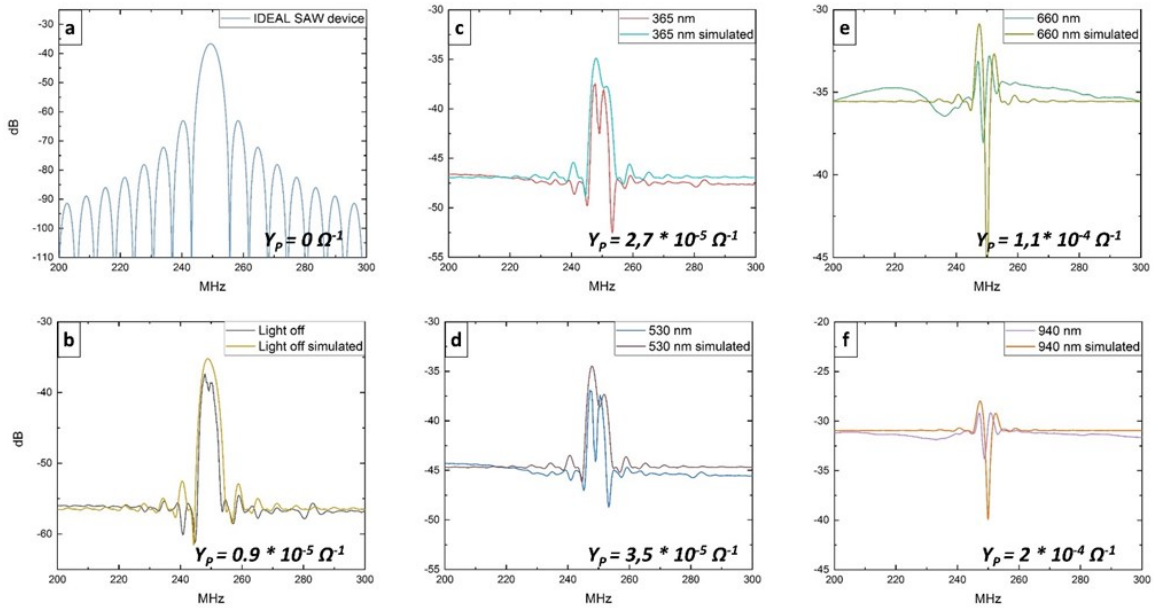

Fig. 3: Experimental and simulated transfer function amplitude S21 of devices fabricated on Silicon substrate: a) Simulated ideal SAW filter without feed-through; b) comparison of experimental and simulated data of device without light stimulus; c,d,e,f) comparison of experimental and simulated data of devices stimulated by 365nm, 530nm, 660nm, 940nm LEDs, respectively.

The resonance frequency has been characterized for all the devices stimulated by different wavelengths. A shift is observed only when the devices have been stimulated by a 365nm light source (Fig. 4) while no resonance shift is observed with the other wavelengths (data not reported in this work). This behavior is due to the large direct bandgap of AlN (around 6 eV) which makes it sensitive in the UV light range (λ<400nm) [19]. In fact, the photoinduced electron screens the piezoelectric field and reduce the acoustic velocity [14]. A larger shift is reported for the Lamb wave on PEN substrate (~60 kHz) compared to the silicon substrate (~20kHz). The larger shift is attributed to the higher resonance frequency of the Lamb wave relative to the Rayleigh wave and not to a higher Lamb wave sensitivity. Noteworthy, the resonance frequency goes back to the initial value after the UV source has been turned off for both resonances. To the best of our knowledge, this is the first detection of UV light with a flexible AlN based SAW device.

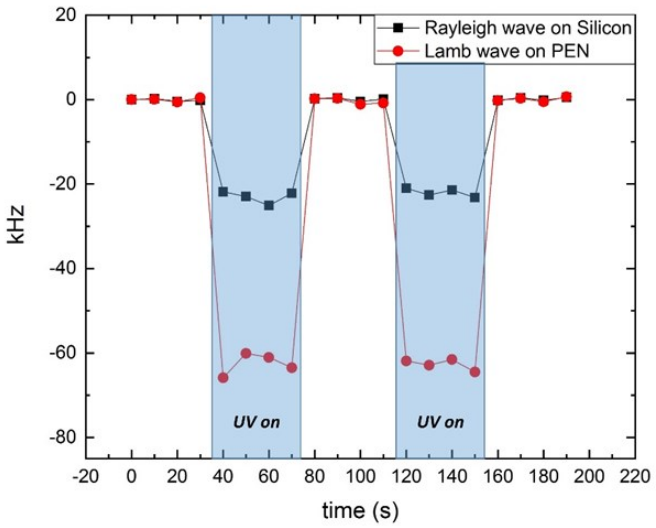

Fig. 4: Real-time shift response of Lamb and Rayleigh frequency modes of ALN- based SAW-based UV detector under 365nm LED source.

VI. Conclusions

The photoresponse of the SAW devices fabricated on silicon and PEN substrate has been investigated. The transfer functions S_{21} are affected significantly when the devices are stimulated by the light. In fact, the devices fabricated on silicon, stimulated by light, showed an enhanced change in the out-of-band signal at near IR while the device fabricated on the PEN flexible substrate does not undergo any variation, suggesting silicon based SAW as an IR sensor. A mathematical model has been implemented to calculate the admittance change as a function of the wavelength light stimulus, achieving an optimal fit for all experimental data. This model, exploited for silicon, could be used for a wide range of semiconductor based SAW devices using different energy bandgap to implement sensitivity for different wavelength. Finally, the Rayleigh and Lamb resonance frequency change has been observed due to the photoinduced electron screens that reduce the acoustic wave velocity when the devices are stimulated by UV light. In particular, the exploitation of PEN based SAW devices enhances the resonance shift improving the responsivity to the UV light.

The knowledge and development of theoretical models and SAW devices sensitive to different power and wavelength light paves the way for a new class of remote device, which could find applications in different fields such as flame monitors, sunlight exposure meters, photochemical phenomena detectors, etc.

References

[1] V. P. Plessky, and L. M. Reindl, "Review on SAW RFID tags," IEEE transactions on ultrasonics, ferroelectrics, and frequency control, vol. 57, no. 3, pp. 654-668, 2010.

[2] A. Pohl, "A review of wireless SAW sensors," IEEE transactions on ultrasonics, ferroelectrics, and frequency control, vol. 47, no. 2, pp. 317-332, 2000.

[3] Y. Q. Fu, J. Luo, N.-T. Nguyen et al., "Advances in piezoelectric thin films for acoustic biosensors, acoustofluidics and lab-on-chip applications," Progress in Materials Science, vol. 89, pp. 31-91, 2017.

[4] G. Iriarte, J. Rodríguez, and F. Calle, "Synthesis of c-axis oriented AlN thin films on different substrates: A review," Materials Research Bulletin, vol. 45, no. 9, pp. 1039-1045, 2010.

[5] L. Lamanna, F. Rizzi, F. Guido et al., "Flexible and Transparent Aluminum‐Nitride‐Based Surface‐Acoustic‐Wave Device on Polymeric Polyethylene Naphthalate," Advanced Electronic Materials, pp. 1900095, 2019.

[6] Y. Ohba, and A. Hatano, "Growth of high-quality AlN and AlN/GaN/AlN heterostructure on sapphire substrate," Japanese journal of applied physics, vol. 35, no. 8B, pp. L1013, 1996.

[7] G. T. Hwang, M. Byun, C. K. Jeong et al., "Flexible Piezoelectric Thin‐Film Energy Harvesters and Nanosensors for Biomedical Applications," Advanced healthcare materials, vol. 4, no. 5, pp. 646-658, 2015.

[8] M. Clement, L. Vergara, J. Sangrador et al., "SAW characteristics of AlN films sputtered on silicon substrates," Ultrasonics, vol. 42, no. 1-9, pp. 403-407, 2004.

[9] Y. A. Vlasov, X.-Z. Bo, J. C. Sturm et al., "On-chip natural assembly of silicon photonic bandgap crystals," Nature, vol. 414, no. 6861, pp. 289, 2001.

[10] P. A. Schultz, "Theory of defect levels and the "band gap problem" in silicon," Physical review letters, vol. 96, no. 24, pp. 246401, 2006.

[11] J. J. Loferski, "Theoretical considerations governing the choice of the optimum semiconductor for photovoltaic solar energy conversion," Journal of Applied Physics, vol. 27, no. 7, pp. 777-784, 1956.

[12] L. Callegaro, Electrical impedance: principles, measurement, and applications: CRC Press, 2012.

[13] Y. Taniyasu, and M. Kasu, "Aluminum nitride deep-ultraviolet light-emitting p–n junction diodes," Diamond and Related Materials, vol. 17, no. 7-10, pp. 1273-1277, 2008.

[14] M. R. Chen, S. Chang, T. C. Chen et al., "Fabrication study of AlN solar‐blind (< 280 nm) MSM photodetectors grown by low‐temperature deposition," physica status solidi (a), vol. 207, no. 1, pp. 224-228, 2010.

[15] K. Rajkanan, R. Singh, and J. Shewchun, "Absorption coefficient of silicon for solar cell calculations," *Solid-State Electronics,* vol. 22, no. 9, pp. 793-795, 1979.

[16] A. Martí, L. Cuadra, and A. Luque, "Quantum dot intermediate band solar cell." pp. 940-943.

[17] S. Kumar, P. Singh, and G. Chilana, "Study of silicon solar cell at different intensities of illumination and wavelengths using impedance spectroscopy," Solar Energy Materials and Solar Cells, vol. 93, no. 10, pp. 1881-1884, 2009.

[18] L. Raniero, E. Fortunato, I. Ferreira et al., "Study of nanostructured/amorphous silicon solar cell by impedance spectroscopy technique," Journal of non-crystalline solids, vol. 352, no. 9-20, pp. 1880-1883, 2006.

[19] C. P. Laksana, M.-r. Chen, Y. Liang et al., "Deep-UVsensors based on SAW oscillators using low-temperature-grown AlN films on sapphires," IEEE transactions on ultrasonics, ferroelectrics, and frequency control, vol. 58, no. 8, pp. 1688-1693, 2011.